U.S. Department of Veterans Affairs
Public Access Author manuscript
Gene Ther. Author manuscript; available in PMC 2019 August 24.

Published in final edited form as:
Gene Ther. 2019 August ; 26(7-8): 308–323. doi:10.1038/s41434-019-0082-7.

AAV-encoded $Ca_V2.2$ peptide aptamer CBD3A6K for primary sensory neuron-targeted treatment of established neuropathic pain

Hongwei Yu[1,2], **Seung Min Shin**[1,2], **Hongfei Xiang**[1,3], **Dongman Chao**[1], **Yongsong Cai**[1,4], **Hao Xu**[1,3], **Rajesh Khanna**[5], **Bin Pan**[1], **Quinn H. Hogan**[1,2]

[1]Department of Anesthesiology, Medical College of Wisconsin, Milwaukee, WI 53226, USA

[2]Zablocki Veterans Affairs Medical Center, Milwaukee, WI 53295, USA

[3]Department of Orthopedic Surgery, Affiliated Hospital of Qingdao University, 266000 Qingdao, PR China

[4]Xi'an Jiaotong University Health Science Center, 710061 Xi'an, Shaanxi, PR China

[5]Departments of Pharmacology, Neuroscience and Anesthesiology, College of Medicine, University of Arizona, Tucson, AZ 85724, USA

Abstract

Transmission of pain signals from primary sensory neurons to secondary neurons of the central nervous system is critically dependent on presynaptic voltage-gated calcium channels. Calcium channel-binding domain 3 (CBD3), derived from the collapsin response mediator protein 2 (CRMP2), is a peptide aptamer that is effective in blocking N-type voltage-gated calcium channel ($Ca_V2.2$) activity. We previously reported that recombinant adeno-associated virus (AAV)-mediated restricted expression of CBD3 affixed to enhanced green fluorescent protein (EGFP) in primary sensory neurons prevents the development of cutaneous mechanical hypersensitivity in a rat neuropathic pain model. In this study, we tested whether this strategy is effective in treating established pain. We constructed AAV6-EGFP-CBD3A6K (AAV6-CBD3A6K) expressing a fluorescent CBD3A6K (replacing A to K at position 6 of CBD3 peptide), which is an optimized variant of the parental CBD3 peptide that is a more potent blocker of $Ca_V2.2$. Delivery of AAV6-CBD3A6K into lumbar (L) 4 and 5 dorsal root ganglia (DRG) of rats 2 weeks following tibial nerve injury (TNI) induced transgene expression in neurons of these DRG and their axonal projections, accompanied by attenuation of pain behavior. We additionally observed that the increased $Ca_V2.2\alpha1b$ immunoreactivity in the ipsilateral spinal cord dorsal horn and DRG following TNI was significantly normalized by AAV6-CBD3A6K treatment. Finally, the increased neuronal activity in the ipsilateral dorsal horn that developed after TNI was reduced by AAV6-CBD3A6K treatment. Collectively, these results indicate that DRG-restricted AAV6 delivery of CBD3A6K is an effective analgesic molecular strategy for the treatment of established neuropathic pain.

Hongwei Yu hyu@mcw.edu.

Conflict of interest The authors declare that they have no conflict of interest.

Introduction

Neuropathic pain following peripheral nerve injury is a devastating problem with limited effective analgesic options, and therefore represents a major unmet health challenge [1, 2]. A common feature of various neuropathic pain conditions is hyperexcitability of pain-signaling primary sensory neurons whose cell bodies are localized in the dorsal root ganglia (DRG) and augmented pain signal transmission at spinal cord level [3–5]. It is well established that N-type calcium channels ($Ca_V2.2$) in nociceptive primary sensory afferents mediate neurotransmitter release at central terminals, including those involved in the increased pain neurotransmission of spinal cord dorsal horn (DH) nociceptive networks [6, 7]. Upregulation of $Ca_V2.2$ in primary sensory neurons contributes to neuropathic pain in multiple models [4, 8–10]. For these reasons, $Ca_V2.2$ channels are major targets of ongoing pharmaceutical research [11–20].

The calcium channel-binding domain 3 (CBD3) is an analgesic peptide aptamer composing of 15 amino acids derived from the collapsin response mediator protein 2 (CRMP2) [21–23]. CRMP2 interaction with $Ca_V2.2\alpha1b$, the pore-forming subunit of $Ca_V2.2$ channels, at the presynaptic afferent terminals promotes neurotransmission, and CBD3 can interrupt this process by interfering with the CRMP2-$Ca_V2.2\alpha1b$ interaction [21, 24]. Application of CBD3 in vivo attenuates pain behaviors in animal models by reducing inward Ca^{2+} currents through the $Ca_V2.2\alpha1b$ subunit via block of its binding to CRMP2 [25, 26]. While effective in providing pain relief, the therapeutic potential of systemic application of CBD3 can be compromised by its short half-life and undesired effects due to broad blockage of the multifunctional $Ca_V2.2$ channels that are distributed throughout the entire body, especially in the central nervous system (CNS) [27]. Since CBD3 exerts its anti-nociceptive effect at the presynaptic terminals of primary sensory neurons [21, 22, 25, 28], we reasoned that restricting distribution of CBD3 to the primary sensory neurons would represent a safer approach to pain therapy. Our previous findings showed that, when delivered *prior* to nerve injury, recombinant adeno-associated viral (AAV)-mediated expression of CBD3 peptide isolated to the peripheral sensory nervous system prevents the development of pain hypersensitivity after peripheral nerve injury [29]. This supports the potential utility of this approach for prophylactic pain therapy. However, whether this targeted genetic therapeutic strategy is efficacious in the more clinical relevant setting of established pain has not been investigated.

A previous study has demonstrated that the CBD3A6K peptide, an optimized variant of the parental CBD3 made by replacing A to K at position 6 of CBD3 peptide, is conformationally rigid compared to original CBD3, thus allowing for a more stable and potent block of $Ca_V2.2$ activity, with greater anti-nociception in pain models [30]. In this study, we constructed a new AAV2/6-EGFP-CBD3A6K vector (AAV6-CBD3A6K) expressing a fluorescent CBD3A6K, which was delivered into the lumbar (L) 4 and 5 DRG after establishment of neuropathic pain. This treatment experimental design is to test the ability of anatomically targeted genetic functional disruption of $Ca_V2.2$ channels in the reversal of established neuropathic pain.

Results

Tibial Nerve Injury (TNI) upregulates $Ca_V2.2\alpha1b$ protein levels in the DRG and spinal cord superficial dorsal horn

In the first series of experiments, the expression of $Ca_V2.2\alpha1b$ was investigated in the L4 and L5 DRG and the corresponding lumbar spinal cord levels by immunoblots and immunohistochemistry (IHC), comparing TNI and control samples. We have previously documented $Ca_V2.2\alpha1b$ immunopositivity in rat DRG sections by IHC using a rabbit polyclonal antibody that is raised against a synthetic peptide corresponding to human $Ca_V2.2\alpha1b$ (amino acids 1857–1950 that have 94% identity to rat $Ca_V2.2\alpha1b$ sequence). In our present immunoblot experiments, the antibody revealed a clean band around ~230 KDa as the target protein of $Ca_V2.2\alpha1b$ in the homogenates prepared from adult rat brain cortex, and preincubation with excess immunogenic peptide eliminated this band in immunoblot (Fig. 1a), which supports the specificity of this antibody for detecting the $Ca_V2.2\alpha1b$ protein expression in rat tissues by immunoblot.

We next quantified $Ca_V2.2\alpha1b$ by immunoblots that separately examined the plasma membrane fraction (PM), identified by enrichment with the sodium/potassium ATPase 1 alpha (NKA1α), compared to the NKA1α-deficient soluble fraction, hereafter referred to as the cytosolic fraction. These were extracted from the pooled L4/L5 DRG tissues followed by immunoblotting of $Ca_V2.2\alpha1b$ protein levels in these fractions. Immunoblot analysis of $Ca_V2.2\alpha1b$ levels in DRG revealed $Ca_V2.2\alpha1b$ protein in both PM and cytosolic fractions (Fig. 1b, c). Four weeks after TNI, $Ca_V2.2\alpha1b$ protein levels were significantly increased in both the PM and the cytosolic fractions, when compared to the corresponding fractions from contralateral DRG (Fig. 1b–d). Increased CRMP2 protein level was also detected in the cytosolic and PM fractions ipsilateral to TNI, compared to controls (Fig. 1b–d). In accordance with these findings, immunohistochemistry revealed an increased profile of $Ca_V2.2\alpha1b$ expression in the TNI-L5 DRG sections compared to controls (Fig. 1e, h).

A line scan function of ImageJ software (http://imagej.nih.gov/ij) was used to compare the alteration of $Ca_V2.2\alpha1b$ immunofluorescent intensity in the ipsilateral vs. contralateral sides of the spinal cord dorsal horn (DH) after TNI [31]. The superficial DH laminae I and II were identified by CGRP and IB4 staining and the border between laminae II and III was identified by staining for protein kinase Cγ (PKCγ), which labels neurons and dense plexus of dendrites of lamina II/III border (Fig. 2a, b) [32, 33]. The average line scan length from the dorsal root entry zone (DREZ) depth to the PKCγ labeled lamina II/III border measured from the cross-sections of lumbar spinal cord (SC) from naïve rats was about 250 μm and defined as the superficial DH, and scan depth from 250 μm onward deeper to 500 μm was arbitrarily defined as the deep DH layers, likely including lamina III–V (Fig. 2c). This DH depth definition by a line scan is similar to a previous report [9]. In the lumbar SC, IHC showed symmetrical $Ca_V2.2\alpha1b$ immunopositivity concentrated in the superficial DH in control rats (Fig. 2d, f). After TNI, an increased profile of $Ca_V2.2\alpha1b$ staining on the ipsilateral side was evident (Fig. 2e, g). Comparing the peak intensity of ipsilateral $Ca_V2.2\alpha1b$ staining (found in the region from DREZ to PKCγ-labeled laminae II inner edge, IIi) normalized against contralateral intensity measured in the same way showed a

significant elevation of this ratio 4 weeks after TNI compared to controls (Fig. 2h). We further found the auxiliary $\alpha_2\delta 1$ subunit of $Ca_V2.2$ was upregulated in the ipsilateral DH after TNI (Fig. 2j, k), which is consistent with prior reports that demonstrated concomitant elevations of $\alpha 2\delta 1$ and $Ca_V2.2\alpha 1b$ protein levels in both the DRG and the central presynaptic terminals following nerve injury or tissue inflammation [4, 20, 34–38].

These results indicate that the protein expression of $Ca_V2.2$ channels in the DRG and spinal cord DH are upregulated following irreversible peripheral nerve injury, which may contribute to the generation of pain after nerve injury [39].

AAV6-CBD3A6K treatment reverses mechanical and cold hypersensitivity

CBD3A6K peptide is an optimized variant of the parental CBD3, made by replacing A to K at position 6 of CBD3 peptide (Fig. 3a). We used a high-throughput approach, probing peptide arrays (~300 peptides) of systematic single site mutants of CBD3 coupled with assessment of binding to $Ca_V2.2$ using a far-Western technique. This limited mutational scans of the CBD3 peptide identified three peptides with point mutations at positions 6 (A6K), 9 (R9L), and 14 (G14F) with greater binding to Ca^{2+} channels than the parent CBD3 peptide [30, 40]. The CBD3A6K peptide resulted in ~80% reduction in capsaicin-evoked blood flow [40], compared to the parental CBD3 peptide which decreased the response to capsaicin by ~64% at similar concentrations [21]. Molecular dynamics simulations revealed a greater propensity of the CBD3A6K to undergo conformational changes implying that this mutant peptide may sample alternative conformational states that are more inclined to bind to the calcium channel and inhibit its interaction with CRMP2 [30].

We next tested whether AAV-mediated CBD3A6K expression selectively in the primary sensory neurons could reverse established neuropathic pain following peripheral nerve injury. We generated AAV vectors expressing EGFP-CBD3A6K or EGFP as the control (Fig. 3b). AAV was packaged into serotype 6 since we have previously demonstrated that this serotype efficiently transduces full-range of DRG neurons [29, 31, 41], which not only express $Ca_V2.2\alpha 1b$ extensively but also appear to increase $Ca_V2.2\alpha 1b$ levels in all sized-neurons after TNI (*cf.* Fig. 1e, g). In the treatment experimental design, the sensitivity to mechanical and cold cutaneous stimulation was assessed prior to and weekly after TNI for 2 weeks. After behavior tests at the 14th day following TNI, rats were randomized to receive intra-ganglionic vector injection of either AAV6-CBD3A6K or AAV6-EGFP, into both the ipsilateral L4 and L5 DRG. Subsequent sensory behavior evaluation was performed on a weekly basis for an additional 6 weeks, after which tissues were harvested for IHC characterization of transgene and target gene expression, and electrophysiological recordings of DH neuronal activity were obtained (see below). The sensory behavior testing before vector injection at the 14th day after TNI was used to evaluate pain behavior development induced by TNI and also as a pain baseline to compare the efficacy post vector treatment [41]. This was based on our previous observations that pain behavior is fully developed at this 2-week timepoint after TNI and persists for at least 8 weeks [41]. It is reported that nearly all of the sciatic DRG perikaryal reside in the L4 and L5 DRG, so these two DRG ipsilateral to TNI were chosen for treatment [41, 42]. Behavioral evaluations showed that all rats established significant pain behaviors 2 weeks after TNI, which included lowered

threshold for withdrawals from mild mechanical stimuli (vF testing, Fig. 4a, b), more frequent hyperalgesic-type responses (sustained lifting, shaking, grooming) after noxious mechanical stimulation (Pin testing, Fig. 4c, d), and more frequent withdrawals from cold (Acetone stimulation) (Fig. 4e, f). These behaviors persisted after injection of the control vector (AAV6-EGFP) during the 6 weeks observation course. In contrast, TNI rats injected with AAV6-CBD3A6K showed gradual reversal of these changes starting about 2 weeks after treatment (Fig. 4). These findings suggest that AAV6-mediated, DRG-targeted CBD3A6K injection has analgesic efficacy in treating established peripheral hypersensitivity in a rat model of neuropathic pain. Notably, sustained analgesic effectiveness was observed for several weeks during the testing course of this study and likely retain longer (Fig. 4).

AAV6-CBD3A6K treatment normalizes $Ca_V2.2\alpha1b$ protein level in the ipsilateral DRG and DH of TNI rats

The in vivo transduction rate for AAV6-CBD3A6K at 8 weeks after TNI and 6 weeks following vector injection was determined by IHC as previously reported [26, 31]. EGFP-positive neurons comprised 45% ± 9% of total neuronal profiles (positive for pan-neuronal marker β3-tubulin, not shown) (n = 3 DRG, five sections per DRG). As we have previously shown [31], transduced DRG neurons included the full size range of the neuronal population that also expressed $Ca_V2.2\alpha1b$ (Fig. 5a–d). Examination of the corresponding SC revealed that EGFP-CBD3A6K fibers terminated throughout the dorsal horn, including in the superficial laminae and in the deeper laminae, as well as in the dorsal columns. No EGFP signal was observed in the intrinsic DH neurons, indicating that AAV did not transverse across synapses (Fig. 5e). Efficient transgene (EGFP and EGFP-CBD3A6K) expression was also verified by Western blots (Fig. 5f). Examination of $Ca_V2.2\alpha1b$ protein levels after AAV6-CBD3A6K treatment revealed reduction of the TNI-induced upregulation of $Ca_V2.2\alpha1b$ in the extracted DRG membrane fractions (Fig. 5g–i). However, TNI-induced upregulation of CRMP2 in DRG was not affected by vector treatment (Fig. 5g–i). Additionally, the injury-induced increase of $Ca_V2.2\alpha1b$ immunostaining in the spinal cord DH was also significantly reversed after AAV6-CBD3A6K treatment (Fig. 6). These results indicate that the analgesic effect of CBD3A6K may be due to reduction of $Ca_v2.2$ channels in the soma membrane and presynaptic terminals of the primary sensory neurons.

AAV6-CBD3A6K treatment normalizes elevated DH neuronal activity in TNI rats

$Ca_V2.2\alpha1b$ is enriched in the central presynaptic terminals of the DH [34–38] and is the major route for presynaptic $Ca2^+$ entry at this synapse, making it necessary for the transmission of nociceptive impulse trains [43, 44]. Peripheral nerve injury results in $Ca_V2.2\alpha1b$ upregulation at the central presynaptic sites of primary afferents, leading to enhanced excitatory signaling in the spinal cord [4, 20]. Our prior examination of animals with TNI-induced neuropathic pain revealed abnormal activity in neurons within lamina IV–VI area of the DH, including elevated responses to mechanical stimulation of peripheral tissues [41]. We therefore examined the effect of DRG treatment with AAV6-CBD3A6K on firing properties of DH neurons after nerve injury. Extracellular recordings of evoked activity were obtained from anesthetized naïve rats, TNI rats without injection, and TNI rats treated with either AAV6-EGFP or AAV6-CBD3A6K injection into the L4 and L5 DRG.

Recordings were performed at a timepoint 8 weeks after TNI and 6 weeks after AAV injection, and focused on the wide dynamic range neurons in laminae IV to VI that were identified by their response to mild and intense mechanical stimuli. These recordings showed the incidence of spontaneous activity was elevated by TNI but was not influenced by vector injections (Fig. 7a), while the firing frequency of this spontaneous activity was not affected by either TNI nor vector injection (Fig. 7b). Identification of the mechanical threshold for firing induced by graded mechanical stimulation during 1 s application of von Frey fibers showed sensitization by nerve injury but recovery towards normal thresholds after the injection of AAV6-CBD3A6K (Fig. 7c). The same change was found using stimulation by a different set of von Frey fibers that were modified by the attachment of 0.1 mm diameter tungsten wire tips to each fiber of the set, in order to produce an area of contact with the skin that did not vary between the fibers with different forces (Fig. 7d). Action potential generation during 10 s sustained force applications (Fig. 7e) showed elevated firing after TNI, which reverted towards normal when the force was applied with either a standard von Frey fiber (26 g with a 1.1 mm diameter tip; Fig. 7f), or with a modified von Frey fiber (16 g with a 0.1 mm diameter tip; Fig. 7g), or during deep mechanical stimulation with an arterial occlusion clamp (Fig. 7h). There were no effects of injury or vector injection observed on the incidence of after-discharges (data not shown).

Discussion

Growing evidence shows that integration of voltage-gated Ca^{2+} channels in a network of protein-interactions is a crucial requirement for proper regulation of channel activity [27, 45]. Presynaptic $Ca_V2.2$ channels, which support synaptic transmission in nociceptive primary sensory neuron axonal terminals, interacts with many other molecules that together comprise the $Ca_V2.2$ interactome [46–53]. Among an increasing number of known interaction partners, CRMP2-$Ca_V2.2$ interaction in the primary sensory neurons and their axonal terminals in the DH has emerged as a critical mechanisms mediating pain signals. Interrupting CRMP2-$Ca_V2.2$ interactions has been demonstrated to be an effective strategy in treatment of pain [21, 25, 26, 28, 54–56]. In the present study, we have extended these observations to a mode of delivery using AAV, which is a promising therapeutic approach, as shown by 176 studies currently registered at the United States National Library of Medicine (https://www.niams.nih.gov/grants-funding/conducting-clinical-research/register-trials-gov). Here, we demonstrate that AAV delivery of the CBD3A6K peptide results in efficient expression in DRG and their central axonal projections, which attenuates sensory hypersensitivity following peripheral nerve injury. Although our study was not designed to confirm the mechanism of analgesic action, our observation that the elevated $Ca_V2.2\alpha1b$ levels in sensory neuronal membrane and ipsilateral DH after injury were substantially reversed by the AAV-CBD3A6K treatment support a mechanism involved reduced binding of $Ca_V2.2\alpha1b$, while the observed reversal of injury-induced DH neuronal hyperactivity supports reduced primary afferent nociceptive neurotransmission as a contributing analgesic process. Overall, our results indicate that DRG-restricted delivery of AAV6-encoded CBD3A6K is an effective analgesic molecular strategy for the treatment of established neuropathic pain in rat.

CRMP2 is upregulated after nerve injury and during the axon regeneration that follows [57–59]. RNA interference of CRMP2 reverses mechanical allodynia induced by peripheral nerve injury in the spare nerve injury (SNI) model [60], indicating that CRMP2 expression is necessary for neuropathic pain. In the present study, we also found that CRMP2 is significantly upregulated in the DRG following peripheral nerve injury and this is accompanied by significantly upregulated $Ca_V2.2\alpha1b$ in both the injured DRG and in the spinal cord DH. CRMP2 plays a key regulatory role in trafficking of $Ca_V2.2\alpha1b$ into the plasma membrane, and afferent central presynaptic enhanced CRMP2-$Ca_V2.2$ interaction increases the quantity of $Ca_V2.2\alpha1b$ proteins at the membrane surface [21, 24, 28]. Therefore, upregulated CRMP2 may play a central role in pathophysiological upregulation of $Ca_V2.2\alpha1b$ intracellular trafficking, resulting in increased calcium channel activity and neuro-transmitter release [24]. Intraganglionic AAV6-CBD3A6K treatment leads to reduction of $Ca_V2.2\alpha1b$ in the DRG neuronal membrane and in the superficial DH. This may indicate that the CBD3A6K analgesic effect is based predominantly on regulating $Ca_V2.2\alpha1b$ trafficking to the sensory neuron membrane rather than $Ca_V2.2\alpha1b$ overall expression.

Our electrophysiological observations show that interruption of CRMP2-$Ca_V2.2\alpha1b$ interactions in primary sensory neurons by AAV6-CBD3A6K treatment reduces injury-induced hyperexcitability of DH neurons in the deep laminae of the dorsal horn during mechanical stimulation. This may well reflect an underlying therapeutic mechanism contributing to the analgesic effect of AAV6-CBD3A6K since the firing activity of these neurons is a feature of various neuropathic pain conditions [61–64]. Moreover, both CRMP2 and $Ca_V2.2\alpha1b$ are expressed in the entire peripheral nervous system, so it can be posited that analgesic effects of AAV-encoded CBD3A6K expression in primary sensory neurons may also be mediated by disruption of $Ca_V2.2\alpha1b$ function at multiple sites along the entire neuron. Finally, it is also possible that CBD3A6K analgesia stems from interfering with T-type voltage gated Ca^{2+} channels, as we and others have reported in the past [29, 30].

Although our findings demonstrate sustained relief of established neuropathic pain from AAV6-mediated CBD3A6K expression in primary sensory neurons, the efficacy is incomplete. Because increased CRMP2 level in the injured DRG persisted after treatment, one of the explanations could be that CRMP2 interacts physically and functionally with multiple molecular nodes that also regulate nociceptive signaling, including sodium channels, sodium-calcium exchanger, and the ligand-gated N-methyl-D-aspartate (NMDA) receptor [65–68]. CRMP2, which is activated by phosphorylation [69], is also a physiological substrate for glycogen synthase kinase 3 (GSK3) and cyclin-dependent kinase 5 (Cdk5), two protein kinases that exhibit greater activity in painful neuropathy [70, 71]. Therefore, the efficacy of CBD3A6K analgesia could be constrained by injury-induced CRMP2 elevation via complex mechanisms in the nociceptive interactome besides $Ca_V2.2$.

For pain gene therapy, it is optimal to have the therapeutic analgesic molecule be delivered only to the pathological tissues and cells [72, 73] in order to reduce the side effects of treatment. DRG are a site in the peripheral somatosensory pathway that is critically involved in the development and maintenance of peripheral nerve injury-induced chronic pain [74–76]. We have shown in this study that genetically disrupting the $Ca_V2.2\alpha1b$-CRMP2

interaction, combined with anatomically restricted AAV-mediated delivery to DRG, can offer a primary sensory neuron-specific approach for analgesia in treatment of painful peripheral neuropathy [29, 41]. In addition, DRG injection has a potential advantage of minimizing antibody formation compared with systemic intravenous injection [77]. Therefore, AAV-mediated DRG-targeted delivery of CBD3A6K has potential to be translated into clinical use for treating patients with neuropathic pain, although long-term safety needs to be further investigated.

In summary, our results indicate that AAV6-mediated DRG-restricted CBD3A6K expression in sensory neurons and their central terminals is an effective analgesic molecular strategy for the treatment of established neuropathic pain. Further development of AAV vector carrying chimeric aptamers or aptamer-siRNA chimeras capable of interfering with multiple CRMP2 downstream nociceptive partners may hold substantial value as a therapeutic target for neuropathic pain.

Materials and methods

Animals

Adult male Sprague Dawley (SD) rats weighing 100–125 g body weight (Charles River Laboratories, Wilmington, MA) were used. All animal experiments were performed with the approval of the Zablocki VA Medical Center Animal Studies Subcommittee and the Medical College of Wisconsin Institutional Animal Care and Use Committee (Permit number: 3690–03) in accordance with the National Institutes of Health Guidelines for the Care and Use of Laboratory Animals. Animals were housed individually in a room maintained at constant temperature (22 ± 0.5 °C) and relative humidity (60 ± 15%) with an alternating 12 h light-dark cycle. Animals were access to water and food ad libitum throughout the experiment, and all efforts were made to minimize suffering. The estimated numbers of animals were derived from our previous experience with similar experiments and the number of experiments needed to achieve statistically significant deviation (20% difference at $p < 0.05$) based on a power analysis [29, 41].

AAV vectors

To construct the AAV vector coding a chimeric EGFPCBD3A6K expression cassette, a DNA fragment encoding a 15mer CBD3A6K peptide was synthesized and subcloned into BsrG I/Sal I sites (Genscript, Piscataway, NJ) of a single-strand AAV expressing plasmid pAAV-CMV-EGFP (Cell Biolabs, San Diego, CA), followed by sequencing confirmation. This generated pAAV-CMV-EGFP-CBD3A6K that codes the EGFP-CBD3A6K fusion protein under the transcriptional control of the CMV promoter. Plasmids pAAV-CMV-EGFP-CBD3A6K and pAAV-CMV-EGFP were used to package AAV2/6-EGFP CBD3A6K, and AAV2/6-EGFP as a control (subsequently referred to as AAV6-CBD3A6K and AAV6-EGFP, respectively) for in vivo injection. AAV vectors were produced and purified in our laboratory by previously described methods [31]. This included AAV particle purification by optiprep ultracentrifugation and concentration by use of Centricon Plus-20 (Regenerated Cellulose 100,000 MWCO, Millipore, Billerica, MA). AAV titer was determined by PicoGreen (life technologies, Carlsbad, CA) assay, and final aliquots were kept in 1×

phosphate buffered saline (PBS) containing 5% sorbitol (Sigma-Aldrich, St. Louis, MO) and stored at −80 °C. The titers of AAV6-CBD3A6K and AAV6-EGFP vectors were 2.01×10^{13} GC/ml and 2.16×10^{13} GC/ml, respectively. The same lots of viral preparations were used for all in vivo experiments.

CBD3 and CBD3A6K structure

The coordinates for the fifteen amino-acid fragment were extracted from chain A of X-ray crystal structure of human CRMP2 (PDB ID 5 mkv) [78]. PyMol (PyMOL Molecular Graphics System, Version 1.8 Schrödinger, LLC) was used to model each peptide using the mutation wizard and choosing the most common rotamer without clashes with adjacent amino acids. The mutated amino acid is shown in red on the peptide structure.

Microinjection of AAV vectors into DRG

AAV vector solution was microinjected into right L4 and L5 DRG using previously described techniques [79]. Briefly, the surgically exposed intervertebral foramen was minimally enlarged by removal of laminar bone. Injection was performed through a micropipette that was advanced ~100 μm into the ganglion. Rats received L4 and L5 DRG injections of either AAV6-CBD3A6K or AAV6-EGFP (one vector per rat), consisting of 2 μl with adjusted titers containing a total of 2.0×10^{10} genome viral particles. Injection was performed over a 5-min period using a microprocessor-controlled injector (Nanoliter 2000, World Precision Instruments, Sarasota, FL, USA). Removal of the pipette was delayed for an additional 5 min to minimize the extrusion of the injectate. Following the injection and closure of overlying muscle and skin, the animals were returned to the animal house where they remained as the designed experiments required.

Tibial nerve injury (TNI)

To model clinical traumatic painful peripheral neuropathy, we performed a TNI, an established model of peripheral nerve injury [41]. Animals were anesthetized using isoflurane at 4% induction and 2% maintenance. Under anesthesia, the right sciatic nerve was exposed under aseptic surgical conditions by blunt dissection of the femoral biceps muscle. The sciatic nerve and its three branches (sural, common peroneal, and tibial nerves) were isolated. The tibial nerve was then tightly ligated and transected distal to the ligation. The overlying muscle and skin were then sutured following surgery. Sham-operated rats were subjected to all preceding procedures without nerve ligation and transection.

Sensory behavioral testing

Behavioral tests were conducted between 9:00 AM and 12:00 AM. Experimenters were blinded to the treatment. Animals were habituated in individual test compartments for at least 1 h before each testing. Behavioral tests, including mechanical withdrawal threshold testing (von Frey), noxious punctate mechanical stimulation (pin test), and cold stimulation, were carried out as previously described [79]. Von Frey test was performed using calibrated monofilaments (Patterson Medical, Bolingbrook, Illinois). Briefly, beginning with the 2.8 g filament, filaments were applied with just enough force to bend the fiber and held for 1 s. If a response was observed, the next smaller filament was applied, and if no response was

observed, the next larger was applied, until a reversal occurred, defined as a withdrawal after a previous lack of withdrawal, or vice versa. Following a reversal event, four more stimulations were performed following the same pattern. The forces of the filaments before and after the reversal, and the four filaments applied following the reversal, were used to calculate the 50% withdrawal threshold [80]. Rats not responding to any filament were assigned a score of 25 g. Punctate mechanical hyperalgesia (Pin test) was determined by gently applying the point of a 22 g spinal anesthesia needle to the center of plantar surface of the hindpaw without penetrating the skin. Five applications were separated by at least 10 s, which was repeated after 2 min, making a total of 10 touches. For each application, the induced behavior was either a very brisk, simple withdrawal with immediate return of the foot to the cage floor, or a sustained elevation with grooming that included licking and chewing, and possibly shaking, which lasted at least 1 s. This latter behavior, termed a hyperalgesic response, is specifically associated with place avoidance [81]. Hyperalgesia was quantified by tabulating hyperalgesia responses as a percentage of total touches. Cold stimulation was performed by expelling acetone from a syringe attached to PE220 tubing to make a meniscus that was touched to the plantar surface of the hind paw, such that the drop spread out on the plantar surface of the paw without contact of the tubing to the skin. Each hind paw was tested 3 times in alternating fashion. Any withdrawal was considered a positive response [79].

Immunohistochemistry and imaging

Staining of paraffin-embedded DRG and spinal cord sections was performed by a standard fluorescent protocol, as previously described [82]. In brief, 5 μm-thick sections were de-paraffinized in xylene and rehydrated through graded alcohols, and treated by heat-induced epitope retrieval in 10 mM citrate buffer, pH 6.0–7.0 (depending on the antibody used). Sections were first immunolabeled with the selected primary antibodies overnight at 4 °C (Table 1). The specificity of the rabbit polyclonal $Ca_V2.2\alpha1b$ antibody (Atlas Antibodies, Stockholm, Sweden), which is raised against a synthetic peptide corresponding to human $Ca_V2.2\alpha1b$ (amino acids 1857–1950 that has 94% identity to rat $Ca_V2.2\alpha1b$ sequence) has been validated showing identification of neuronal $Ca_V2.2\alpha1b$ immunopositive profile in DRG by a previous publication [83]. The specificities of the other antibodies used in this study have been previously confirmed and illustrated the specificities of antigens detection [29, 31, 82]. All antibodies were diluted in 1× phosphate buffered saline (PBS), containing 0.05% Triton X-100 and 3% bovine serum albumin (BSA). Normal immunoglobulin G (IgG from same species as the first antibody, Table 1) was replaced for the first antibody as the negative controls. The appropriate fluorophore-conjugated (Alexa 488 or Alexa 594, 1:2000) secondary antibodies (Jackson ImmunoResearch, West Grove, PA) were used to reveal immune complexes. The sections were washed three times 5 min each with PBS containing 0.05% tween-20 between incubations. To stain nuclei, 1.0 μg/ml Hoechst33342 (Hoechst, ThermoFisher) was added to the secondary antibody mixture. The sections were examined and images acquired on a Nikon TE2000-S fluorescence microscope (El Segundo, CA), equipped with an Optronics QuantiFire digital camera and acquisition software (Ontario, NY), as well as filters suitable for selectively detecting the green, red and blue fluorescence. For each comparative experiment, all images were acquired with identical settings for detector gain and under a 10× objective (0.5 numerical aperture at 2048 × 2048 pixel

resolution) or 20× objective (0.3 numerical aperture at 1024 × 1024 pixel resolution). Some IHC images were captured under a Nikon C1 digital eclipse confocal microscope. For double-label colocalization, images from the same section but showing different antigen signals were overlaid.

$Ca_V2.2\alpha1b$ immunofluorescent intensity was quantified and compared between the ipsilateral and contralateral sides in the dorsal horn of lumbar spinal cord cross sections from control and TNI animals using ImageJ as described previously [31]. In brief, the fluorescence intensity values of ipsilateral and contralateral sides were acquired along a line positioned between the dorsal root entry zone (DREZ), defining the entry surface of primary afferent into the spinal cord [84], and the central canal in the contralateral and ipsilateral sides of the section (Line scan function, scan width 100 pixels in width and 500 μm in length). The peak intensity across the full length of this line was then determined for each section. The average peak intensity of $Ca_V2.2\alpha1b$ staining in the DH was compared between the ipsilateral and contralateral sides.

Immunoblots

The lysates from tissues and cultured cells were extracted using 1× RIPA buffer (20 mm Tris-HCl pH 7.4, 150 mm NaCl, 1% Nonidet P-40, 1% sodium deoxycholate, 0.1% SDS, with 0.1% Triton X100 and protease inhibitor cock-tail). To examine the subcellular localization of the target protein, DRG tissues were fractionated to obtain sodium/potassium-ATPase (NKA1α) enriched plasma membrane and NKA1α-eliminated cytosol fractions using the ProteoExtract Subcellular Proteome Extraction Kit (Millipore), which contains extraction buffers with ultra-pure chemicals to ensure high reproducibility, protease inhibitor cocktail to prevent protein degradation and benzonase nuclease to remove contaminating nucleic acids, according to the manufacturer's instructions. Protein concentration was determined by using the Pierce BCA kit (ThermoFisher). Equivalent protein samples were size separated using 10% or 4–20% SDS-PAGE gels (Bio-Rad Laboratories, Des Plaines, IL), transferred to 0.22 μm nitrocellulose membranes, and blocked for 1 h in 5% skim milk. The blots were subsequently incubated overnight at 4 °C with appropriate antibodies. To verify the band specificity of $Ca_V2.2\alpha1b$ detection using a rabbit $Ca_V2.2\alpha1b$ antibody, the antibody solution was preincubated with the specific $Ca_V2.2\alpha1b$ antigenic peptides (5 μg/ml, Atlas antibodies) for 2 h prior to immunoblotting. Immunoreactive proteins were detected by Pierce enhanced chemiluminescence (ThermoFisher) after incubation for 1 h with HRP-conjugated second antibodies (1:5000, Bio-Rad). Densitometry of bands of interests was analyzed using ImageJ v.1.46. Ratios of the band density of the target proteins to the sum of Tubb3 and NKA1α band density were calculated and the percentage changes of target proteins in the experimental samples compared with those from the control samples [83, 85].

In vivo recording of DH neuron activity

Rats were initially anesthetized with 2% isoflurane, and then were injected with 1.2 g/kg urethane subcutaneously. During recording, the isoflurane will be discontinued or run at levels of ≤0.2% such that the rats will remain immobile but metabolically and hemodynamically stable, which are confirmed by arterial blood analysis with a blood gas

analyzer (ABL800FLEX, Radiometer, Copenhagen, Denmark), and continuous blood pressure was monitoring via a carotid artery PE-10 cannula. A heating pad was used to maintain body temperature at 37 °C. For extracellular DH neuronal recordings, a laminectomy was performed from the T13 to the L3 vertebrae to expose the mid-lumbar spinal cord, and a stabilizing stereotaxic clamp was applied to the spinal process rostral to the exposure. The dura was opened, and the cord was covered in warm mineral oil. A single barreled glass micropipette filled with solution containing KCl (2 mM) was advanced into the spinal cord using a microdrive, targeting lamina IV to VI of the L4 to L5 level at depths of 400–700 μm from the cord surface. Wide dynamic range neurons that responded to nonnoxious and noxious stimulation in a graded manner were selected for study. Sequentially, the ipsilateral hindpaw was stimulated using a standard set of graded von Frey fibers applied for 1 s to determine the threshold for response to punctate mechanical stimulation, then stroking with a brush to evoke dynamic mechanical stimulation, then application of von Frey fibers modified by attaching uniform tungsten tips (0.1 mm) to identify the threshold for response to noxious mechanical stimulation, then application of a 26 g von Frey fiber (tip diameter 1.1 mm) for 10 s to determine firing rate, then application of a 16 g modified von Frey fiber (tip diameter 0.1 mm) for 10 s to determine firing rate, then application of a Dieffenbach bulldog clamp for 10 s to determine firing rate during deep mechanical stimulation. Electrophysiological signals were collected with an Axon Axoclamp 900 A microelectrode amplifier (Molecular Devices, San Jose, CA), filtered at 1 kHz, and sampled at 10 kHz using a digitizer (DigiData 1440 A). Action potentials were isolated by setting the threshold above background noise, and individual units were identified by template matching using Spike2 (Cambridge Electronic Design Limited, Cambridge, UK) or pClamp 11 (Molecular Devices).

Statistics

Statistical analysis was performed with GraphPad PRISM 6 (GraphPad Software, San Diego, CA). Behavioral changes over treatment baseline and between groups for von Frey measurements were generated using repeated measures twoway ANOVA and post-hoc analysis with Bonferroni test. Pin and cold test results in discrete numerical data without normal distribution so conservative nonparametric analysis were performed by Friedman's test for analysis of variance and Dunn's test for post-hoc analysis. The differences of the targeted gene expression by immunoblots and ImageJ line analysis were compared with one-way ANOVA, two-tailed unpaired *t*-test. Results are reported as mean and standard deviation of mean (SEM). For electrophysiological data, the effect of nerve injury by TNI was determined by comparison to findings in naïve animals with Mann–Whitney nonparametric *t*-test, and the effect of the two vectors was compared to non-injected TNI animals using nonparametric Kruskal–Wallis ANOVA with Dunn's test for paired comparisons. $p < 0.05$ were considered statistically significant.

Acknowledgements

This research was supported by a grant from the Department of Veterans Affairs Rehabilitation Research and Development I01RX001940 (to Q. Hogan). R. Khanna is supported by grants from National Institutes of Health Awards (1R01NS098772 and 1R01DA042852). H. Xiang was a recipient of National Natural Science Foundation of China (81802190, 81772412). Y. Cai was a recipient of Chinese Scholarship Council.

References

1. Dzau VJ, Pizzo PA. Relieving pain in America: insights from an Institute of Medicine committee. JAMA 2014;312:1507–8. 10.1001/jama.2014.12986 [PubMed: 25321905]
2. Loeser JD. Relieving pain in America. Clin J Pain 2012;28:185–6. 10.1097/AJP.0b013e318230f6c1 [PubMed: 22290333]
3. Basbaum AI, Bautista DM, Scherrer G, Julius D. Cellular and molecular mechanisms of pain. Cell 2009;139:267–84. 10.1016/j.cell.2009.09.028 [PubMed: 19837031]
4. Costigan M, Scholz J, Woolf CJ. Neuropathic pain: a maladaptive response of the nervous system to damage. Annu Rev Neurosci 2009;32:1–32. 10.1146/annurev.neuro.051508.135531 [PubMed: 19400724]
5. Campbell JN, Meyer RA. Mechanisms of neuropathic pain. Neuron 2006;52:77–92. 10.1016/j.neuron.2006.09.021 [PubMed: 17015228]
6. Bucci G, Mochida S, Stephens GJ. Inhibition of synaptic transmission and G protein modulation by synthetic CaV2.2 Ca(2)+ channel peptides. J Physiol 2011;589:3085–101. 10.1113/jphysiol.2010.204735 [PubMed: 21521766]
7. Bell TJ, Thaler C, Castiglioni AJ, Helton TD, Lipscombe D. Cell-specific alternative splicing increases calcium channel current density in the pain pathway. Neuron 2004;41:127–38. [PubMed: 14715140]
8. Altier C, Dale CS, Kisilevsky AE, Chapman K, Castiglioni AJ, Matthews EA, et al. Differential role of N-type calcium channel splice isoforms in pain. J Neurosci 2007;27:6363–73. 10.1523/JNEUROSCI.0307-07.2007 [PubMed: 17567797]
9. Bauer CS, Nieto-Rostro M, Rahman W, Tran-Van-Minh A, Ferron L, Douglas L, et al. The increased trafficking of the calcium channel subunit alpha2delta-1 to presynaptic terminals in neuropathic pain is inhibited by the alpha2delta ligand pregabalin. J Neurosci 2009;29:4076–88. 10.1523/JNEUROSCI.0356-09.2009 [PubMed: 19339603]
10. Ji RR, Strichartz G. Cell signaling and the genesis of neuropathic pain. Sci STKE 2004;2004:reE14 10.1126/stke.2522004re14 [PubMed: 15454629]
11. Tyagarajan S, Chakravarty PK, Park M, Zhou B, Herrington JB, Ratliff K, et al. A potent and selective indole N-type calcium channel (Ca(v)2.2) blocker for the treatment of pain. Bioorg Med Chem Lett 2011;21:869–73. 10.1016/j.bmcl.2010.11.067 [PubMed: 21195616]
12. Liang M, Yin XL, Shi HB, Li CY, Li XY, Song NY, et al. Bilirubin augments Ca(2+) load of developing bushy neurons by targeting specific subtype of voltage-gated calcium channels. Sci Rep 2017;7:431 10.1038/s41598-017-00275-9 [PubMed: 28348377]
13. Norton RS, McDonough SI. Peptides targeting voltage-gated calcium channels. Curr Pharm Des 2008;14:2480–91. [PubMed: 18781996]
14. Perret D, Luo ZD. Targeting voltage-gated calcium channels for neuropathic pain management. Neurotherapeutics 2009;6:679–92. 10.1016/j.nurt.2009.07.006 [PubMed: 19789072]
15. Pexton T, Moeller-Bertram T, Schilling JM, Wallace MS. Targeting voltage-gated calcium channels for the treatment of neuropathic pain: a review of drug development. Expert Opin Investig Drugs 2011;20:1277–84. 10.1517/13543784.2011.600686
16. Vink S, Alewood PF. Targeting voltage-gated calcium channels: developments in peptide and small-molecule inhibitors for the treatment of neuropathic pain. Br J Pharmacol 2012;167:970–89. 10.1111/j.1476-5381.2012.02082.x [PubMed: 22725651]
17. Zamponi GW. Targeting voltage-gated calcium channels in neurological and psychiatric diseases. Nat Rev Drug Discov 2016;15:19–34. 10.1038/nrd.2015.5 [PubMed: 26542451]
18. Park J, Luo ZD. Calcium channel functions in pain processing. Channels 2010;4:510–7. [PubMed: 21150297]
19. Patel R, Montagut-Bordas C, Dickenson AH. Calcium channel modulation as a target in chronic pain control. Br J Pharmacol 2018;175:2173–84. 10.1111/bph.13789 [PubMed: 28320042]
20. McGivern JG. Targeting N-type and T-type calcium channels for the treatment of pain. Drug Discov Today 2006;11:245–53. 10.1016/S1359-6446(05)03662-7 [PubMed: 16580601]

21. Brittain JM, Duarte DB, Wilson SM, Zhu W, Ballard C, Johnson PL, et al. Suppression of inflammatory and neuropathic pain by uncoupling CRMP-2 from the presynaptic Ca(2)(+) channel complex. Nat Med 2011;17:822–9. 10.1038/nm.2345 [PubMed: 21642979]
22. Moutal A, Wang Y, Yang X, Ji Y, Luo S, Dorame A, et al. Dissecting the role of the CRMP2-neurofibromin complex on pain behaviors. Pain 2017;158:2203–21. 10.1097/j.pain.0000000000001026 [PubMed: 28767512]
23. Hoppe-Seyler F, Crnkovic-Mertens I, Tomai E, Butz K. Peptide aptamers: specific inhibitors of protein function. Curr Mol Med 2004;4:529–38. [PubMed: 15267224]
24. Brittain JM, Piekarz AD, Wang Y, Kondo T, Cummins TR, Khanna R. An atypical role for collapsin response mediator protein 2 (CRMP-2) in neurotransmitter release via interaction with presynaptic voltage-gated calcium channels. J Biol Chem 2009;284:31375–90. 10.1074/jbc.M109.009951 [PubMed: 19755421]
25. Francois-Moutal L, Wang Y, Moutal A, Cottier KE, Melemedjian OK, Yang X, et al. A membrane-delimited N-myristoylated CRMP2 peptide aptamer inhibits CaV2.2 trafficking and reverses inflammatory and postoperative pain behaviors. Pain 2015;156:1247–64. 10.1097/j.pain.0000000000000147 [PubMed: 25782368]
26. Xie JY, Chew LA, Yang X, Wang Y, Qu C, Wang Y, et al. Sustained relief of ongoing experimental neuropathic pain by a CRMP2 peptide aptamer with low abuse potential. Pain 2016;157:2124–40. 10.1097/j.pain.0000000000000628 [PubMed: 27537210]
27. Simms BA, Zamponi GW. Neuronal voltage-gated calcium channels: structure, function, and dysfunction. Neuron 2014;82:24–45. 10.1016/j.neuron.2014.03.016 [PubMed: 24698266]
28. Chi XX, Schmutzler BS, Brittain JM, Wang Y, Hingtgen CM, Nicol GD, et al. Regulation of N-type voltage-gated calcium channels (Cav2.2) and transmitter release by collapsin response mediator protein-2 (CRMP-2) in sensory neurons. J Cell Sci 2009;122:4351–62. 10.1242/jcs.053280 [PubMed: 19903690]
29. Fischer G, Pan B, Vilceanu D, Hogan QH, Yu H. Sustained relief of neuropathic pain by AAV-targeted expression of CBD3 peptide in rat dorsal root ganglion. Gene Ther 2014;21:44–51. 10.1038/gt.2013.56 [PubMed: 24152582]
30. Piekarz AD, Due MR, Khanna M, Wang B, Ripsch MS, Wang R, et al. CRMP-2 peptide mediated decrease of high and low voltage-activated calcium channels, attenuation of nociceptor excitability, and anti-nociception in a model of AIDS therapy-induced painful peripheral neuropathy. Mol Pain 2012;8:54 10.1186/1744-8069-8-54 [PubMed: 22828369]
31. Yu H, Fischer G, Ferhatovic L, Fan F, Light AR, Weihrauch D, et al. Intraganglionic AAV6 results in efficient and long-term gene transfer to peripheral sensory nervous system in adult rats. PLoS ONE 2013;8:e61266 10.1371/journal.pone.0061266 [PubMed: 23613824]
32. Hughes DI, Scott DT, Todd AJ, Riddell JS. Lack of evidence for sprouting of Abeta afferents into the superficial laminas of the spinal cord dorsal horn after nerve section. J Neurosci 2003;23:9491–9. [PubMed: 14573528]
33. Yu H, Pan B, Weyer A, Wu HE, Meng J, Fischer G, et al. CaMKII controls whether touch is painful. J Neurosci 2015;35:14086–102. 10.1523/JNEUROSCI.1969-15.2015 [PubMed: 26490852]
34. D'Arco M, Margas W, Cassidy JS, Dolphin AC. The upregulation of alpha2delta-1 subunit modulates activity-dependent Ca2+signals in sensory neurons. J Neurosci 2015;35:5891–903. 10.1523/JNEUROSCI.3997-14.2015 [PubMed: 25878262]
35. Lu SG, Zhang XL, Luo ZD, Gold MS. Persistent inflammation alters the density and distribution of voltage-activated calcium channels in subpopulations of rat cutaneous DRG neurons. Pain 2010;151:633–43. 10.1016/j.pain.2010.08.030 [PubMed: 20884119]
36. Hoppa MB, Lana B, Margas W, Dolphin AC, Ryan T. A. alpha2delta expression sets presynaptic calcium channel abundance and release probability. Nature 2012;486:122–5. 10.1038/nature11033 [PubMed: 22678293]
37. Westenbroek RE, Hell JW, Warner C, Dubel SJ, Snutch TP, Cat-terall WA. Biochemical properties and subcellular distribution of an N-type calcium channel alpha 1 subunit. Neuron 1992;9:1099–115. [PubMed: 1334419]

38. Cizkova D, Marsala J, Lukacova N, Marsala M, Jergova S, Orendacova J, et al. Localization of N-type Ca2+ channels in the rat spinal cord following chronic constrictive nerve injury. Exp Brain Res 2002;147:456–63. 10.1007/s00221-002-1217-3 [PubMed: 12444477]
39. Todd AJ. Neuronal circuitry for pain processing in the dorsal horn. Nat Rev Neurosci 2010;11:823–36. 10.1038/nrn2947 [PubMed: 21068766]
40. Wilson SM, Brittain JM, Piekarz AD, Ballard CJ, Ripsch MS, Cummins TR, et al. Further insights into the antinociceptive potential of a peptide disrupting the N-type calcium channel-CRMP-2 signaling complex. Channels 2011;5:449–56. 10.4161/chan.5.5.17363 [PubMed: 21829088]
41. Xiang H, Liu Z, Wang F, Xu H, Roberts C, Fischer G, et al. Primary sensory neuron-specific interference of TRPV1 signaling by AAV-encoded TRPV1 peptide aptamer attenuates neuropathic pain. Mol Pain 2017;13:1744806917717040 10.1177/1744806917717040
42. Swett JE, Torigoe Y, Elie VR, Bourassa CM, Miller PG. Sensory neurons of the rat sciatic nerve. Exp Neurol 1991;114:82–103. [PubMed: 1915738]
43. Heinke B, Balzer E, Sandkuhler J. Pre- and postsynaptic contributions of voltage-dependent Ca2+channels to nociceptive transmission in rat spinal lamina I neurons. Eur J Neurosci 2004;19:103–11. [PubMed: 14750968]
44. Rycroft BK, Vikman KS, Christie MJ. Inflammation reduces the contribution of N-type calcium channels to primary afferent synaptic transmission onto NK1 receptor-positive lamina I neurons in the rat dorsal horn. J Physiol 2007;580:883–94. 10.1113/jphysiol.2006.125880 [PubMed: 17303639]
45. Chai Z, Wang C, Huang R, Wang Y, Zhang X, Wu Q, et al. CaV2.2 gates calcium-independent but voltage-dependent secretion in mammalian sensory neurons. Neuron 2017;96:1317–26. 10.1016/j.neuron.2017.10.028.e1314 [PubMed: 29198756]
46. Zhang FX, Gadotti VM, Souza IA, Chen L, Zamponi GW. BK potassium channels suppress cavalpha2delta subunit function to reduce inflammatory and neuropathic pain. Cell Rep 2018;22:1956–64. 10.1016/j.celrep.2018.01.073 [PubMed: 29466724]
47. Bezprozvanny I, Zhong P, Scheller RH, Tsien RW. Molecular determinants of the functional interaction between syntaxin and N-type Ca2+ channel gating. Proc Natl Acad Sci USA 2000;97:13943–8. 10.1073/pnas.220389697 [PubMed: 11087812]
48. Cassidy JS, Ferron L, Kadurin I, Pratt WS, Dolphin AC. Functional exofacially tagged N-type calcium channels elucidate the interaction with auxiliary alpha2delta-1 subunits. Proc Natl Acad Sci USA 2014;111:8979–84. 10.1073/pnas.1403731111 [PubMed: 24889613]
49. Diverse-Pierluissi M, Dunlap K. Interaction of convergent pathways that inhibit N-type calcium currents in sensory neurons. Neuroscience 1995;65:477–83. [PubMed: 7777162]
50. Kadurin I, Rothwell SW, Lana B, Nieto-Rostro M, Dolphin AC. LRP1 influences trafficking of N-type calcium channels via interaction with the auxiliary alpha2delta-1 subunit. Sci Rep 2017;7:43802 10.1038/srep43802 [PubMed: 28256585]
51. Leroy J, Richards MW, Butcher AJ, Nieto-Rostro M, Pratt WS, Davies A, et al. Interaction via a key tryptophan in the I-II linker of N-type calcium channels is required for beta1 but not for palmitoylated beta2, implicating an additional binding site in the regulation of channel voltage-dependent properties. J Neurosci 2005;25:6984–96. 10.1523/JNEUROSCI.1137-05.2005 [PubMed: 16049174]
52. Omote K, Kawamata M, Satoh O, Iwasaki H, Namiki A. Spinal antinociceptive action of an N-Type voltage-dependent calcium channel blocker and the synergistic interaction with morphine. Anesthesiology 1996;84:636–43. [PubMed: 8659792]
53. Sheng ZH, Rettig J, Cook T, Catterall WA. Calcium-dependent interaction of N-type calcium channels with the synaptic core complex. Nature 1996;379:451–4. 10.1038/379451a0 [PubMed: 8559250]
54. Ju W, Li Q, Allette YM, Ripsch MS, White FA & Khanna R. Suppression of pain-related behavior in two distinct rodent models of peripheral neuropathy by a homopolyarginine-conjugated CRMP2 peptide. J Neurochem 10.1111/jnc.12070 (2012).
55. Ripsch MS, Ballard CJ, Khanna M, Hurley JH, White FA, Khanna R. A Peptide uncoupling crmp-2 from the presynaptic ca(2+) channel complex demonstrates efficacy in animal models of

migraine and aids therapy-induced neuropathy. Transl Neurosci 2012;3:1–8. 10.2478/s13380-012-0002-4 [PubMed: 22662308]

56. Ip JP, Fu AK, Ip NY. CRMP2: functional roles in neural development and therapeutic potential in neurological diseases. Neuroscientist 2014;20:589–98. 10.1177/1073858413514278 [PubMed: 24402611]
57. Suzuki Y, Nakagomi S, Namikawa K, Kiryu-Seo S, Inagaki N, Kaibuchi K, et al. Collapsin response mediator protein-2 accelerates axon regeneration of nerve-injured motor neurons of rat. J Neurochem 2003;86:1042–50. [PubMed: 12887701]
58. Kamiya Y, Saeki K, Takiguchi M. CDK5, CRMP2 and NR2B in spinal dorsal horn and dorsal root ganglion have different role in pain signaling between neuropathic pain model and inflammatory pain model. Eur J Anaesthesiol 2013;30:214.
59. Zhang JN, Koch JC. Collapsin response mediator protein-2 plays a major protective role in acute axonal degeneration. Neural Regen Res 2017;12:692–5. 10.4103/1673-5374.206631 [PubMed: 28616018]
60. Moutal A, Luo S, Largent-Milnes TM, Vanderah TW, Khanna R. Cdk5-mediated CRMP2 phosphorylation is necessary and sufficient for peripheral neuropathic pain. Neurobiol Pain In press, 10.1016/j.ynpai.2018.1007.1003 (2018).
61. Chapman V, Suzuki R, Dickenson AH. Electrophysiological characterization of spinal neuronal response properties in anaesthetized rats after ligation of spinal nerves L5-L6. J Physiol 1998;507:881–94. [PubMed: 9508847]
62. Takaishi K, Eisele JH Jr., Carstens E. Behavioral and electro-physiological assessment of hyperalgesia and changes in dorsal horn responses following partial sciatic nerve ligation in rats. Pain 1996;66:297–306. [PubMed: 8880853]
63. Palecek J, Paleckova V, Dougherty PM, Carlton SM, Willis WD. Responses of spinothalamic tract cells to mechanical and thermal stimulation of skin in rats with experimental peripheral neuropathy. J Neurophysiol 1992;67:1562–73. 10.1152/jn.1992.67.6.1562 [PubMed: 1321241]
64. Laird JM, Bennett GJ. An electrophysiological study of dorsal horn neurons in the spinal cord of rats with an experimental peripheral neuropathy. J Neurophysiol 1993;69:2072–85. 10.1152/jn.1993.69.6.2072 [PubMed: 8394412]
65. Brustovetsky T, Pellman JJ, Yang XF, Khanna R, Brustovetsky N. Collapsin response mediator protein 2 (CRMP2) interacts with N-methyl-D-aspartate (NMDA) receptor and Na+/Ca2+exchanger and regulates their functional activity. J Biol Chem 2014;289:7470–82. 10.1074/jbc.M113.518472 [PubMed: 24474686]
66. Dustrude ET, Wilson SM, Ju W, Xiao Y, Khanna R. CRMP2 protein SUMOylation modulates NaV1.7 channel trafficking. J Biol Chem 2013;288:24316–31. 10.1074/jbc.M113.474924 [PubMed: 23836888]
67. Brittain JM, Pan R, You H, Brustovetsky T, Brustovetsky N, Zamponi GW, et al. Disruption of NMDAR-CRMP-2 signaling protects against focal cerebral ischemic damage in the rat middle cerebral artery occlusion model. Channels (Austin) 2012;6:52–59. [PubMed: 22373559]
68. Kanellopoulos AH, Koenig J, Huang H, Pyrski M, Millet Q, Lolignier S, et al. Mapping protein interactions of sodium channel NaV1.7 using epitope-tagged gene-targeted mice. Embo J 2018;37:427–45. 10.15252/embj.201796692 [PubMed: 29335280]
69. Sumi T, Imasaki T, Aoki M, Sakai N, Nitta E, Shirouzu M, et al. Structural insights into the altering function of CRMP2 by phosphorylation. Cell Struct Funct 2018;43:15–23. 10.1247/csf.17025 [PubMed: 29479005]
70. Wilson SM, Ki Yeon S, Yang XF, Park KD, Khanna R. Differential regulation of collapsin response mediator protein 2 (CRMP2) phosphorylation by GSK3ss and CDK5 following traumatic brain injury. Front Cell Neurosci 2014;8:135 10.3389/fncel.2014.00135 [PubMed: 24904280]
71. Brittain JM, Wang Y, Eruvwetere O, Khanna R. Cdk5-mediated phosphorylation of CRMP-2 enhances its interaction with CaV2.2. FEBS Lett 2012;586:3813–8. 10.1016/j.febslet.2012.09.022 [PubMed: 23022559]
72. Bolash RB, Niazi T, Kumari M, Azer G, Mekhail N. Efficacy of a targeted drug delivery on-demand bolus option for chronic pain. Pain Pract 2018;18:305–13. 10.1111/papr.12602 [PubMed: 28520273]

73. Hayek SM, Sweet JA, Miller JP, Sayegh RR. Successful management of corneal neuropathic pain with intrathecal targeted drug delivery. Pain Med 2016;17:1302–7. 10.1093/pm/pnv058 [PubMed: 26814286]
74. Berta T, Qadri Y, Tan PH, Ji RR. Targeting dorsal root ganglia and primary sensory neurons for the treatment of chronic pain. Expert Opin Ther Targets 2017;21:695–703. 10.1080/14728222.2017.1328057 [PubMed: 28480765]
75. Guha D, Shamji MF. The dorsal root Ganglion in the pathogenesis of chronic neuropathic pain. Neurosurgery 2016;63:118–26. 10.1227/NEU.0000000000001255 [PubMed: 27399376]
76. Hogan QH. Labat lecture: the primary sensory neuron: where it is, what it does, and why it matters. Reg Anesth Pain Med 2010;35:306–11. 10.1097/AAP.0b013e3181d2375e [PubMed: 20460965]
77. Terashima T, Ogawa N, Nakae Y, Sato T, Katagi M, Okano J, et al. Gene therapy for neuropathic pain through siRNA-IRF5 gene delivery with homing peptides to microglia. Mol Ther Nucleic Acids 2018;11:203–15. 10.1016/j.omtn.2018.02.007 [PubMed: 29858055]
78. Zheng Y, Sethi R, Mangala LS, Taylor C, Goldsmith J, Wang M, et al. Tuning microtubule dynamics to enhance cancer therapy by modulating FER-mediated CRMP2 phosphorylation. Nat Commun 2018;9:476 10.1038/s41467-017-02811-7 [PubMed: 29396402]
79. Fischer G, Kostic S, Nakai H, Park F, Sapunar D, Yu H, et al. Direct injection into the dorsal root ganglion: technical, behavioral, and histological observations. J Neurosci Methods 2011;199:43–55. [PubMed: 21540055]
80. Chaplan SR, Bach FW, Pogrel JW, Chung JM, Yaksh TL. Quantitative assessment of tactile allodynia in the rat paw. J Neurosci Methods 1994;53:55–63. [PubMed: 7990513]
81. Wu HE, Gemes G, Zoga V, Kawano T, Hogan QH. Learned avoidance from noxious mechanical simulation but not threshold semmes weinstein filament stimulation after nerve injury in rats. J Pain 2010;11:280–6. 10.1016/j.jpain.2009.07.011 [PubMed: 19945356]
82. Yu H, Fischer G, Jia G, Reiser J, Park F, Hogan QH. Lentiviral gene transfer into the dorsal root ganglion of adult rats. Mol Pain 2011;7:63. [PubMed: 21861915]
83. Liu Z, Wang F, Fischer G, Hogan QH & Yu H. Peripheral nerve injury induces loss of nociceptive neuron-specific Galphai-interacting protein in neuropathic pain rat. Mol Pain 10.1177/1744806916646380 (2016).
84. Ramer MS, Duraisingam I, Priestley JV, McMahon SB. Two-tiered inhibition of axon regeneration at the dorsal root entry zone. J Neurosci 2001;21:2651–60. [PubMed: 11306618]
85. Xiang H, Xu H, Fan F, Shin SM, Hogan QH & Yu H. Glial fibrillary acidic protein promoter determines transgene expression in satellite glial cells following intraganglionic adeno-associated virus delivery in adult rats. J Neurosci Res 10.1002/jnr.24183 (2017).

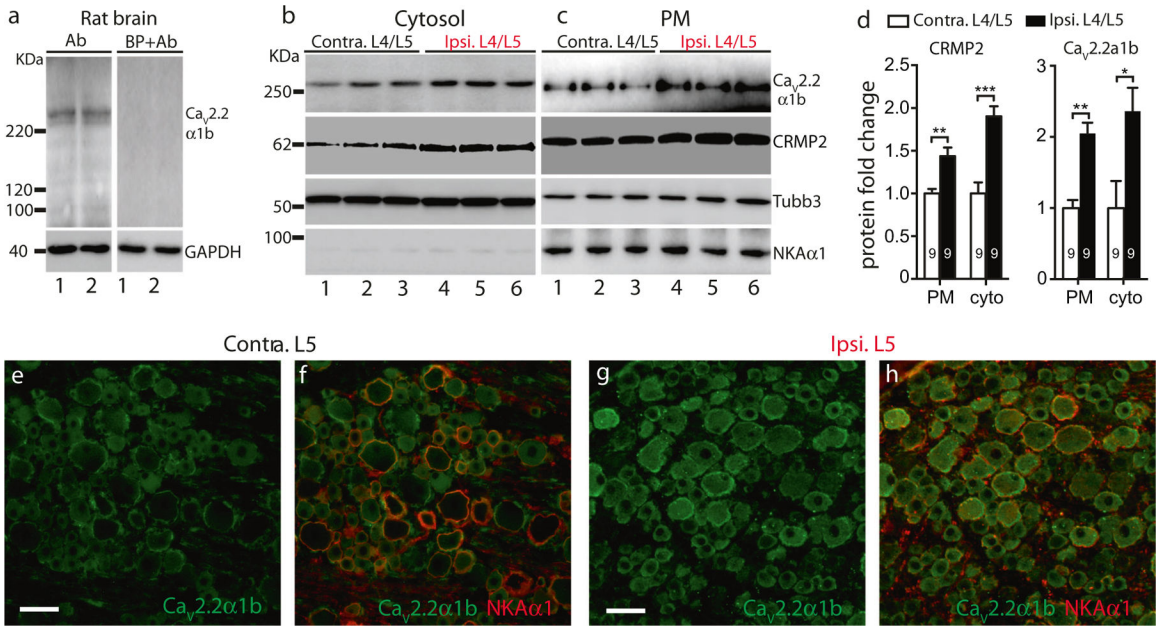

Fig. 1.

$Ca_V2.2\alpha1b$ protein expression is significantly increased in the lumbar DRG following TNI. Immunoblot reveals a clean band around ~230 KDa of $Ca_V2.2\alpha1b$ protein in the homogenate of rat brain cortex (**a**, left panel), and preincubation with excess immunogenic peptide completely eliminated this band (**a**, right panel). The NKA1α-deficient cytosolic fraction and NKA1α-enriched plasma membrane (PM) fraction were extracted from the DRG tissues at 4 weeks after TNI, and subjected to immunoblotting as shown in the representative immunoblots of $Ca_V2.2\alpha1b$, CRMP2, Tubb3, and NKA1α of cytosol (**b**) and PM fractions (**c**), respectively. Bar charts (**d**) show densitometry analysis of immunoblots. The number in each bar is the number of analyzed DRG per group. *, **, and *** denote $p < 0.05$, $p < 0.01$, and $p < 0.001$, respectively (Two tailed unpaired Student's *t*-test). Representative montage images show immunostaining of $Ca_V2.2\alpha1b$ (green) and colabeling with NKA1α (red) in the merged image from the DRG sections of control (**e, f**) and TNI rat (**g, h**). Scale bar: 100 μm for all IHC images

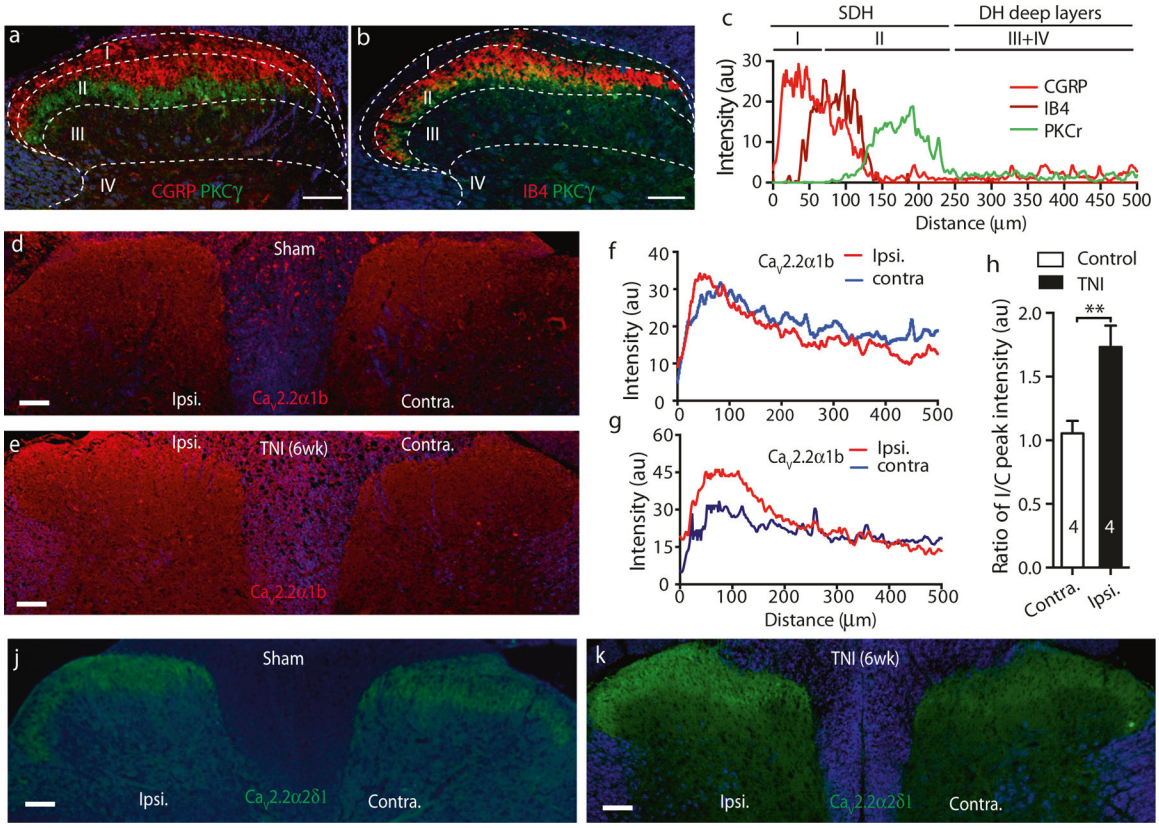

Fig. 2.

$Ca_V2.2\alpha1b$ protein expression is significantly increased in the lumbar DH following TNI. PKCγ colabeling with CGRP (**a**) or IB4 (**b**) followed by ImageJ line scan analysis (**c**) delineates the profiles and length of superficial DH (laminae I and II) and deeper layers of the DH (laminae III and IV). $Ca_V2.2\alpha1b$ immunoreactive (IR) staining (red) in the DH of control animal shows symmetrical intensity (**d**), which is confirmed by line scans (**f**). In contrast, $Ca_V2.2\alpha1b$-IR intensity in the ipsilateral (ipsi.) DH of TNI rats appears increased compared to contralateral (contra.) side (**e**), which is verified by line scans (**g**). The effect of TNI is further confirmed by analysis of the ratio of peak intensities (ipsi./contra, **h**) (Two-tailed unpaired Student's *t*-test). Numbers in each bar represents the spinal cords analyzed from each group. In parallel, control spinal DH shows symmetrical immunostaining intensity of the $Ca_V2.2$ auxiliary subunit $\alpha2\delta1$ ($Ca_V2.2\alpha2\delta1$), while the $Ca_V2.2\alpha2\delta1$ level is apparently increased on the ipsilateral side compared to contralateral side in the TNI rat. Scale bar: 100 μm for all IHC images. ** $p < 0.01$

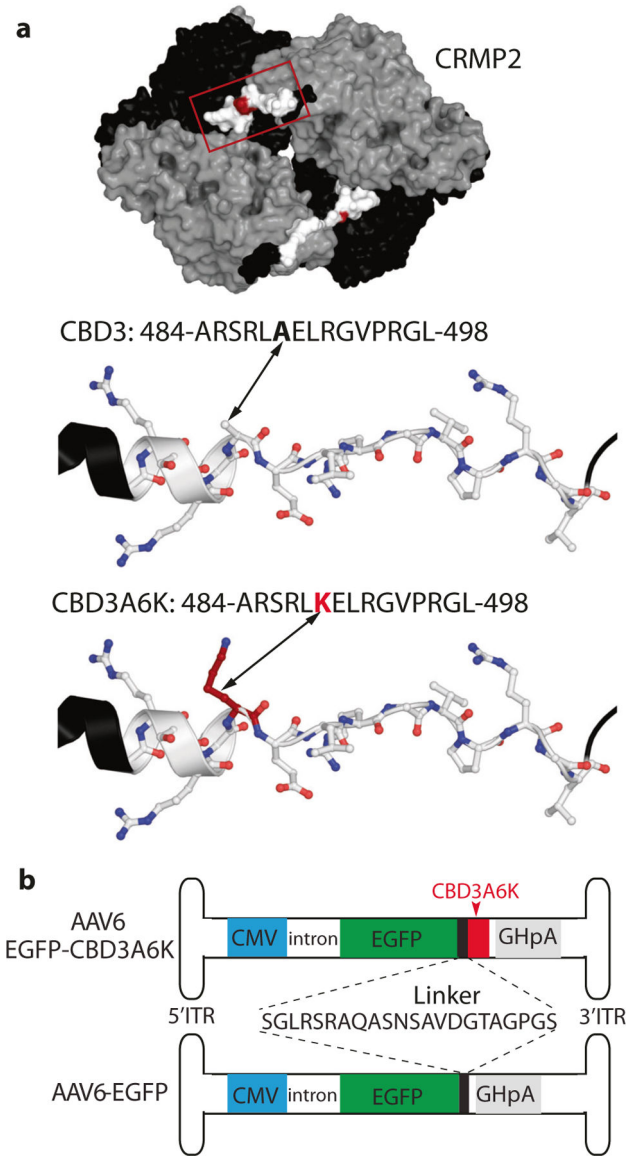

Fig. 3.

Structure of CRMP2 and CDB3/CBD3A6K peptides and AAV constructs. **a** X-ray crystal structure of human CRMP2 (PDB ID 5 mkv) (top panel) [78]. CBD3 residues are shown as sticks (white) and flanking amino acids in black. Inset: Tetrameric CRMP2 with chains A and D in black. Red box outlines location of CBD3 peptide in white with A484 in red. Reader visible CBD3 (middle panel) and CBDA6K (bottom panel) structures are shown as ribbons and arrowheads point to A6 (while) of CBD3 or K6 (red) of CBD3A6K. **b** Schematic outline of AAV vectors. The vector genomes of AAV6-EGFPCBD3A6K and AAV6-EGFP are flanked by AAV2 inverted terminal repeats (ITR). Transgene cassettes encode EGFP-CBD3A6K separated by a 22aa linker between EGFP and CBD3A6K or EGFP-linker alone down-stream of a chimeric intron enhancing transcription driven by the cytomegalovirus (CMV) promoter, and contain polyadenylation signal element from the

human growth hormone (GHpA). The amino acid the linker sequence is shown in the middle of two vectors

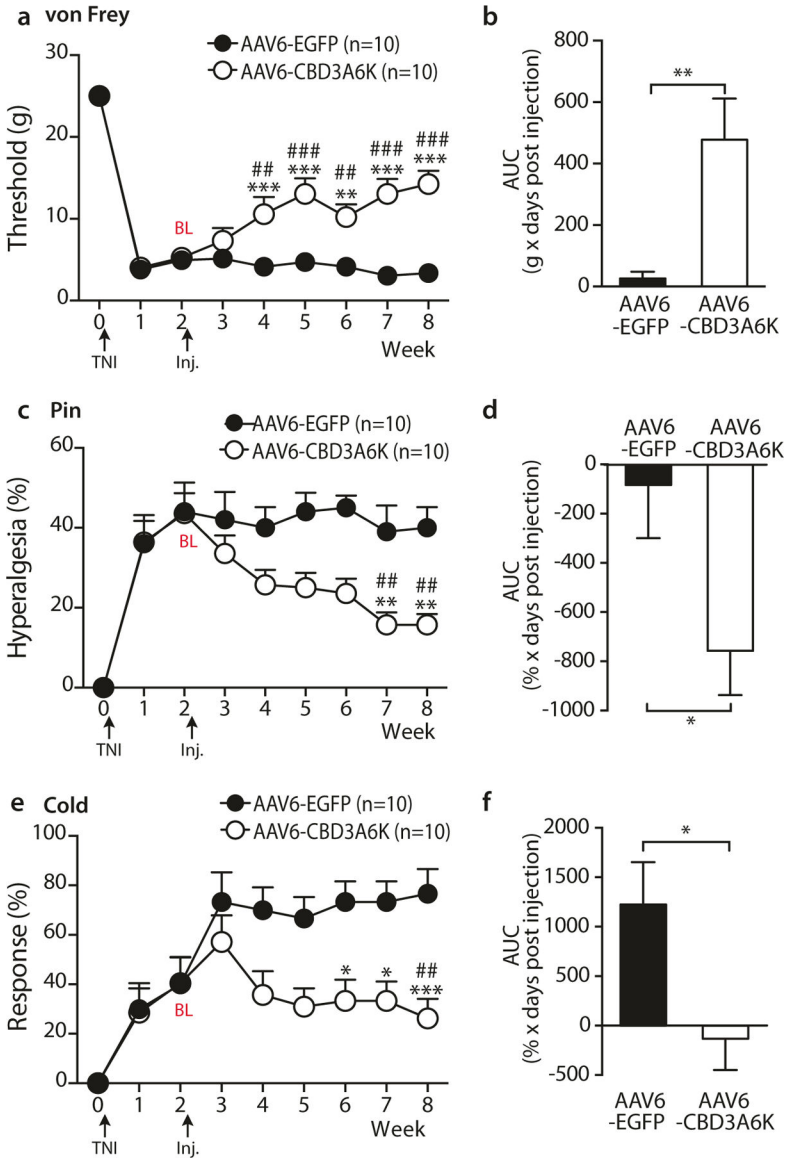

Fig. 4.

Intraganglionic AAV6-CBD3A6K treatment alleviates TNI-induced pain behavior. Left panels show the time courses for the group averages of sensitivity to innocuous punctate mechanical stimulation (von Frey, **a**), hyperalgesia behavior after touch with a pin (Pin, c), and sensitivity to acetone stimulation (Cold, **e**) before and after DRG injection of either AAV6-EGFP (filled circle, $n = 10$ rats) or AAV6-CBD3A6K (empty circles, $n = 10$ rats). Injection of AAV vectors into the fourth and fifth lumbar DRG was performed 2-week after tibial nerve injury (TNI) immediately after the week-2 behavior determinations. Right panels show averaged area under the curve (AUC) calculated for each individual for the time period following vector injection for von Frey (**b**), pin (**d**), and cold (**f**). Behavior tests before AAV injection at 2-week after TNI were used as the treatment baseline values (BL) for AUC calculation. $*p < 0.05$, $**p < 0.01$, and $***p < 0.001$ for comparison to treatment baseline (BL) and $^{\#}p < 0.05$, $\#\#p < 0.01$, and $^{\#\#\#}p < 0.001$ for comparison between groups after

treatment, respectively (**a, c, e;** repeated measures two-way ANOVA and post-hoc analysis with Bonferroni test for von Frey and nonparametric analyses by Friedman's test with Dunn's post-hoc for Pin and Cold). *$p < 0.05$, **$p < 0.01$ for AUC comparison between groups (**b, d, f,** two-tailed unpaired Student's *t*-tests)

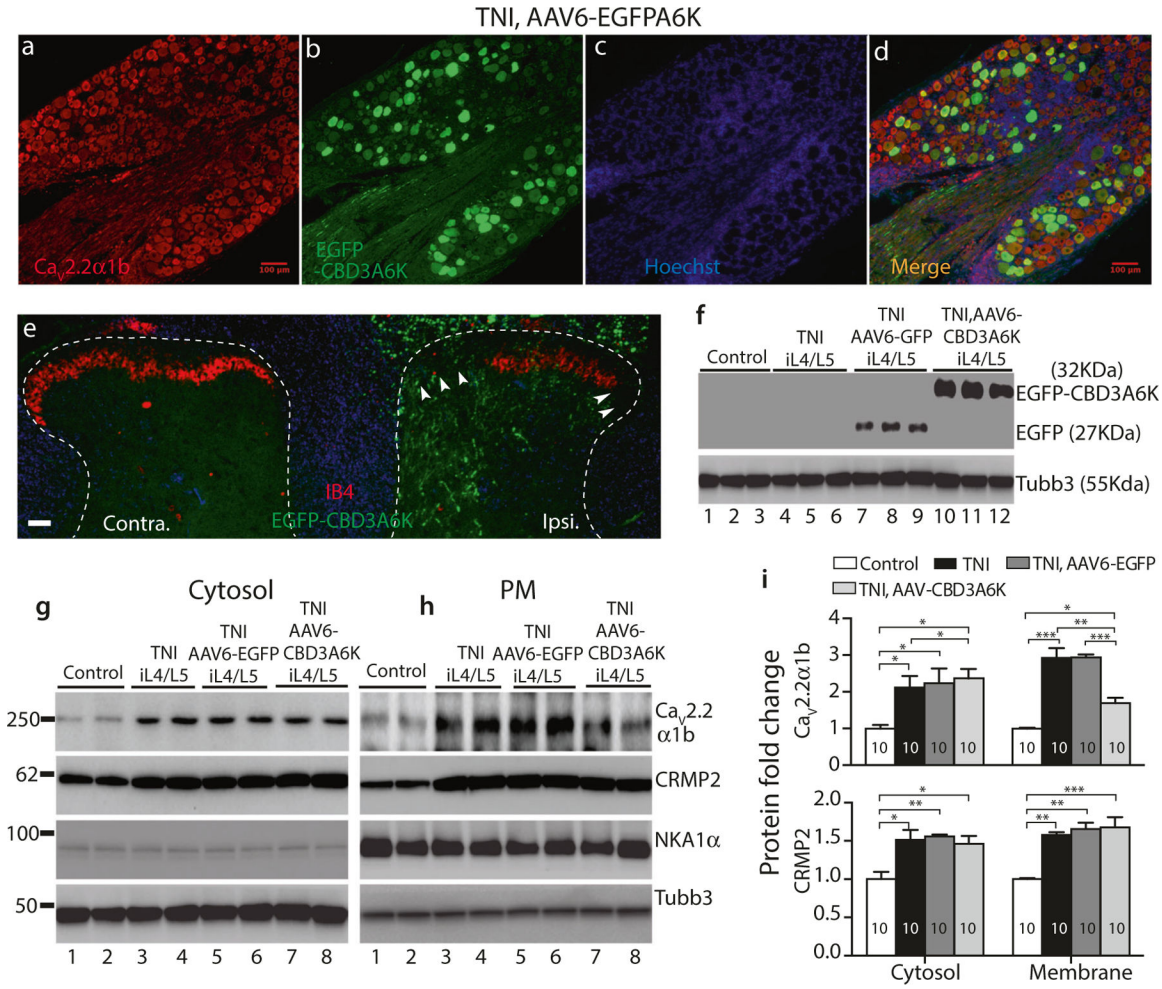

Fig. 5.

AAV6-CBD3A6K treatment reverses increased Ca$_V$2.2α1b protein level in DRG. Representative montage IHC images show profiles of immunolabeling of Ca$_V$2.2α1b (**a**), EGFP-tagged CBD3A6K 6 weeks after AAV6-CDD3A6K treatment (**b**), Hoechst nuclear staining (**c**), and colabeling of Ca$_V$2.2α1b and EGFP-tagged CBD3A6K in the merged image (**d**) on a ipsilateral L5 DRG section from TNI rat. EGFP-tagged CBD3A6K distributes in the afferent central terminals of the TNI ipsilateral DH (**e**) with abolished IB4 staining in the tibial nerve central terminal zone (arrowheads). Western blots verifies transgenes (EGFP and EGFP-CBD3A6K) expression in DRG 6 weeks after vector injection, showing EGFP-CBD3A6K band ~5 KDa larger than EGFP (**f**). Representative immunoblots of Ca$_V$2.2α1b, CRMP2, NKA1α, and Tubb3 on the cytosol (**g**) and PM fractions (**h**) extracted from control and TNI only DRG, as well as the TNI DRG after vector treatment, as indicated, respectively. Bar charts (**i**) show densitometry analysis of immunoblots, $*p < 0.05$, $**p < 0.01$, and $***p < 0.001$ for comparison of Ca$_V$2.2α1b and CRMP2 protein level in the cytosol and PM fractions in each group (One-way ANOVA analysis of variance with Turkey post-hoc test). The number in each bar is the number of analyzed DRG per group. Scale bar: 100 μm for all IHC images

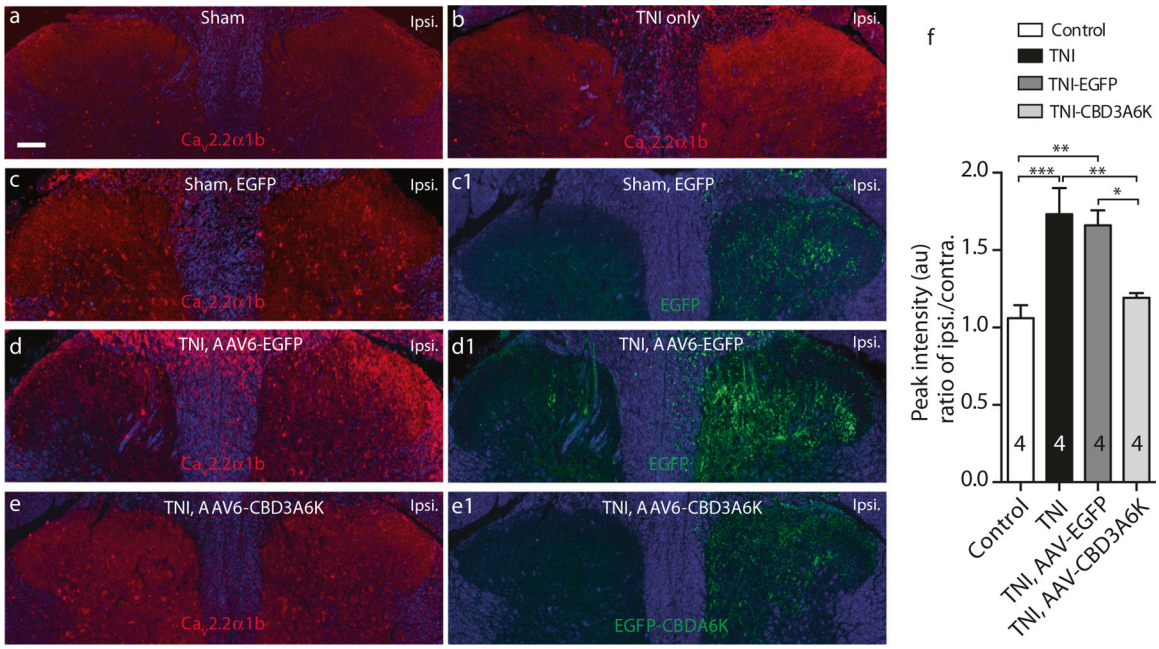

Fig. 6.

AAV6-CBD3A6K treatment normalizes Ca$_V$2.2α1b upregulation in the DH. Representative images show profiles of immunolabeling of Ca$_V$2.2α1b in the DH from control (**a**) and TNI only (**b**), control colabeled Ca$_V$2.2α1b (**c**) with EGFP (**c1**) after AAV6-EGFP injection, TNI colabeled Ca$_V$2.2α1b (**d**) with EGFP (**d1**) after AAV6-EGFP injection, and TNI colabeled Ca$_V$2.2α1b (**e**) with EGFP (**e1**) after AAV6-CBD3A6K injection. Comparison of the ratios of ipsi-lateral/contralateral peak intensity (au) in control, TNI only, TNI with AAV6-EGFP injection, and TNI with AAV6-CBD3A6K treatment by ImageJ line scan function was analyzed (**f**). *, **, and *** denote $p < 0.05$, $p < 0.01$, and $p < 0.001$, respectively (One-way ANOVA with Turkey post-hoc analysis). Scale bar: 100 μm for all IHC images

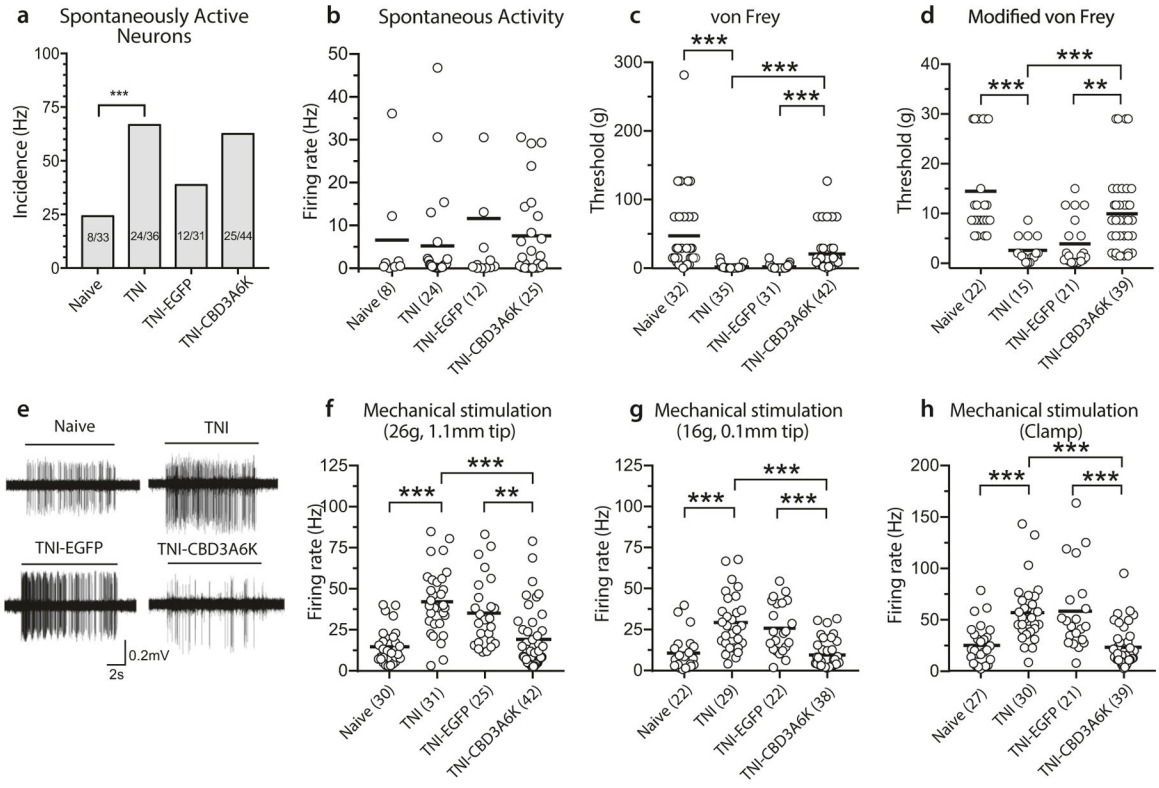

Fig. 7.

AAV6-CBD3A6K treatment reverses elevated mechanosensory-induced firing of DH neurons after TNI. Recording from wide dynamic range neurons in the DH of anesthetized rats shows elevated incidence of spontaneous activity 8 weeks after tibial nerve injury (TNI group) compared to naive animals, and no effects on the incidence of spontaneous activity 6 weeks after vector injection into DRG L4 and L5 of the AAV6-EGFP vector (labeled as the TNI-EGFP group) or the AAV6-CBD3A6K (the TNI-CBD3A6K group) (**a**). In contrast, the threshold for triggering DH neuronal firing during mechanical stimulation with von Frey fibers (**b**) is decreased by TNI, and is reversed towards normal by vector injection in the TNI-CBD3 group, while the control vector had no effect (TNI-EGFP group). Similar results are found with mechanical stimulation using von Frey fibers with standardized 0.1 mm tips (**c**). Firing rates were then measured during 10 s sustained mechanical stimulation (**d**, sample traces using 26 g von Frey, 1.1. mm tip), which showed increased firing after TNI, with reversal towards normal after treatment in the TNI-CBD3 group (**e**). Similar effects of sensitization with TNI and reversal by therapeutic vector injection were found using mechanical stimulation with regular von Frey (26 g, 1.1 mm tip, **f**) and modified von Frey (16 g, 0.1 mm tip; g) or with an arterial compression clamp (**h**) Numbers in parentheses represents the number of cells recorded. *$p < 0.05$, **$p < 0.01$, and ***$p < 0.001$ (One-way ANOVA analysis of variance with Turkey post-hoc test)

Table 1

Primary antibodies and IgG controls used in this study

Antibody[a]	Host	Supplier/Catalog#[b]	Dilution
EGFP	Mouse monoclonal	SCB/ sc-9996	1:100 (IHC), 1:400 (Wb)
IB4		ThermoFisher/I21413	1.0 μg/ml
$Ca_V2.2\alpha 1b$	Rabbit polyclonal	Atlas AB/HPA044347	1:100 (IHC), 1:400 (Wb)
$Ca_V2.2\alpha 2\delta 1$	Mouse monoclonal	Sigma/D219	1:100 (IHC)
CGRP	Mouse monoclonal	SCB/sc-57053	1:500 (IHC)
NKA1α	Mouse monoclonal	SCB/sc48345	1:400 (IHC and Wb)
PKCγ	Rabbit polyclonal	SCB/sc-211	1:100 (IHC)
Tubb3	Mouse monoclonal	SCB/sc-80016	1:400 (IHC), 1:1000 (Wb)
CRMP2	Rabbit polyclonal	Sigma/C2993	1:500 (Wb)
IgG control	Mouse	LF/31903	1:100–400
IgG control	Rabbit	LF/MA5–16384	1:100–1000

[a]Antibody abbreviations: CaV2.2α1b, voltage-dependent N-type calcium channel subunit alpha-1B; CaV2.2α2δ1, voltage-dependent calcium channel subunit alpha-2/delta-1; CGRP, Calcitonin gene related peptide; PKCγ, Protein kinase C gamma; Tubb3, β3-Tubulin; NKA1α, Sodium/potassium ATPase 1 alpha; CRMP2, collapsin response mediator protein 2.

[b]SCB, Santa Cruz Biotechnology, Santa Cruz, CA; ThermoFisher, Pittsburgh, PA; Atlas AB, Atlas Antibodies, Stockholm, Sweden; Sigma, Sigma-Aldrich, St Louis, MO; Life Technologies, Carlsbad, CA